WILEY

Bayesian approaches for evaluating wind-resistant performance of long-span bridges using structural health monitoring data

Y.W. Wang[1,2] | Y.Q. Ni[1,2] | Q.H. Zhang[1,2] | C. Zhang[1,2]

[1]Department of Civil and Environmental Engineering, The Hong Kong Polytechnic University, Hung Hom, Kowloon, Hong Kong

[2]National Rail Transit Electrification and Automation Engineering Technology Research Center (Hong Kong Branch), The Hong Kong Polytechnic University, Hung Hom, Kowloon, Hong Kong

Correspondence
Y.Q. Ni, Department of Civil and Environmental Engineering, The Hong Kong Polytechnic University, Hung Hom, Kowloon, Hong Kong.
Email: ceyqni@polyu.edu.hk

Summary
Reliable estimation of wind-induced displacement responses of long-span bridges is critical to evaluating their wind-resistant performance. In this study, two Bayesian approaches, Bayesian generalized linear model (BGLM) and sparse Bayesian learning (SBL), are proposed for characterizing the wind-induced lateral displacement responses of long-span bridges with structural health monitoring (SHM) data. They are fully model-free data-driven approaches, preferable for reckoning the wind-induced total displacement intended for wind-resistant performance assessment. With the measured displacement responses and wind speeds, a BGLM is developed to characterize the nonlinear relationship between the total displacement response and wind speed, where the Bayesian model class selection (BMCS) criterion is incorporated to determine the optimal model. In the model formulation by SBL, both wind speed and wind direction are treated as explanatory variables to elicit a probabilistic model with sparse structure. The SBL cleverly makes the resulting model to exempt from overfitting and generalizes well on unseen data. The two formulated models are then utilized to forecast the wind-induced displacement responses in extreme typhoon events beyond the monitoring scope, and the predicted displacement responses are contrasted to the finite element analysis results and the design maximum allowable displacement under the serviceability limit state (SLS). The proposed methods are demonstrated using the monitoring data acquired by GPS sensors and anemometers instrumented on a long-span suspension bridge. The results show that the SBL model is superior to the BGLM for wind-induced displacement response prediction and is amenable to SHM-based evaluation of wind-resistant performance under extreme typhoon conditions.

KEYWORDS
Bayesian generalized linear model, long-span bridge, sparse Bayesian learning, structural health monitoring, wind-resistant performance

1 | INTRODUCTION

Long-span bridges are vital components of transportation networks, whose failure can dramatically affect local transport services and cause substantial economic losses and major casualties. Bridge dynamic displacement response is a significant metric in bridge performance assessment. In particular, long-span cable-supported bridges are flexible and sensitive to wind, whose main girder displacement response can reach a plateau under strong aerostatic and fluctuating wind actions. According to the aerostatic response analysis on the Sutong Bridge (a cable-stayed bridge with a main span of 1088 m) by Xu et al.,[1] the lateral displacement response of the main girder can approach 1.2 m under the strong wind speed of 40 m/s at the attack angle of 0°. The buffeting analysis on the Golden Gate Bridge[2] showed that the maximum displacement response of the main span can reach 1.7 m under the wind speed of 31 m/s. Such large amplitude of displacement response would threaten the safety of the whole bridge.[3] For instance, the old Tacoma Narrows Bridge in Washington State collapsed under winds of approximately 18 m/s due to violent torsional oscillations.[4]

Theoretical exploration, numerical simulation, and wind tunnel tests have been conducted in an attempt to comprehend the lateral displacement response of long-span bridges. Cheng and Xiao[5] proposed a simplified method for evaluating lateral response that takes into account geometric nonlinearity and the three components of displacement-dependent wind loads. Chan[6] formulated a structural health monitoring system (SHMS)-refined finite element model for buffeting analysis of a long-span bridge and compared the computed buffeting-induced displacement with the measurement results. Kwon et al.[7] conducted buffeting analysis for the catwalk structure of a suspension bridge and evaluated the lateral displacement response through wind tunnel tests. However, accurate prediction of displacement response for a complex long-span bridge by theoretical exploration, numerical simulation, and wind tunnel tests is still a challenge on account of the inappropriate ignorance of some subordinate factors, imprecise assignment of initial parameters, uncertain boundary conditions, and so on.[3]

In the past two decades, with the rapid development of structural health monitoring (SHM) technology, it has been feasible to deploy various sensors to collect the authentic structural behaviors under actual environmental and load actions. As part of a typical SHM system, the Global Positioning System (GPS) technique has been widely used to monitor the dynamic response of bridge structures, which has an advantage to reliably measure the absolute 3D quasi-static and dynamic displacements. The earliest trial use of GPS for monitoring long-span bridges under wind loads was made on the Humber Bridge in 1996.[8] After this successful trial, many subsequent applications were reported worldwide, and a number of long-span bridges have incorporated GPS into their long-term SHM systems.[9–11] For example, the Akashi Kaikyo Bridge (a suspension bridge with a main span of 1991 m) in Japan was equipped with GPS on the tower top and in the middle span for displacement monitoring.[9] In Hong Kong, a GPS system was added later to the Wind And Structural Health Monitoring System (WASHMS) deployed on the Tsing Ma Bridge (a suspension bridge with a main span of 1377 m), Kap Shui Mun Bridge (a cable-stayed bridge with a main span of 430 m), and Ting Kau Bridge (a cable-stayed bridge with two main spans of 448 and 475 m, respectively) to monitor the displacement responses of bridge towers, cables, and decks.[10] In the mainland China, a number of long-span bridges have been equipped with SHM systems inclusive of GPS for monitoring displacement response, such as the Humen Bridge,[12] the Sutong Bridge,[13] and Shandong Binzhou Yellow River highway bridge.[14]

Research efforts have been made on correlation regularity between the bridge lateral displacement response and wind speed by use of SHM data, and it turns out that the relationship between the response and wind speed is nonlinear.[3,15,16] In all the previous studies, however, the correlation models were formulated with deterministic model parameters which were estimated by statistical analysis of a large amount of SHM data. A serious flaw of this modeling approach is that the accuracy of estimated model parameters is affected by the data volume, limited data without sufficient coverage leading to inaccurate results. More importantly, the formulated models fail to account for uncertainty inherent in the monitoring data and interpret the model error. Bayesian approaches, on the other hand, offer an appealing alternative in that (i) they treat model parameters as random variables rather than deterministic quantities and therefore accommodate uncertainty contained in the monitoring data and (ii) they enable the quantification of model error and prediction uncertainty.[17] In the Bayesian context, a prior belief about the model parameters is conferred; then the monitoring data are used to update their belief in the posterior distribution. The Bayesian posterior distribution offers a lot more flexibility in the type of evidence and provides information more transparent to interpret. Although Bayesian approaches have been widely used in different engineering fields,[18–31] no study has been attempted on developing a Bayesian approach to probabilistically characterize the correlation between the wind speed and wind-induced bridge response for wind-resistant performance assessment.

This study is therefore focused on exploring the nonlinear relationship between the lateral displacement response of a bridge and the corresponding wind speed/direction by use of SHM data and Bayesian inference and then evaluating the wind-resistant performance of bridge in the Bayesian context. The basic rationale behind this study is that, as the lateral displacement responses of a bridge under the action of wind loads are reflective of its wind-resistant performance, the wind-resistant performance can be evaluated using the correlation regularity between the lateral displacement response and wind speed/direction. More specifically, the abnormal variation of the correlation indicates a deterioration in the wind-resistant performance. The primary contribution of this paper is twofold: (i) we propose Bayesian generalized linear model (BGLM) to probabilistically formulate the nonlinear relationship between the lateral displacement response and wind speed, where the Bayesian model class selection (BMCS) criterion is employed to determine the optimal BGLM in multitudinous candidate models; and (ii) we propose sparse Bayesian learning (SBL) to formulate a probabilistic model of the lateral displacement response versus wind speed and wind direction and compare it with BGLM in terms of the capability to predict the bridge response under extreme winds. The rest of the paper is organized as follows. Section 2 presents the BGLM and the SBL. In Section 3, the proposed methods are illustrated and verified using the real-world monitoring data collected from a long-span suspension bridge under typhoons of different scales. Conclusions are drawn in Section 4.

2 | METHODOLOGY

2.1 | Bayesian generalized linear model

2.1.1 | BGLM

The generalized linear model (GLM) is a flexible generalization of ordinary linear regression that allows for response variables that have other than a normal distribution. Suppose that there are n sets of independent observations $\{(y_i, x_i), i = 1, \cdots, n\}$, where y_i's are the response variables and x_i's are the explanatory variables, and the relationship between them is expressed as the following nonlinear function

$$
\begin{aligned}
y_i = \beta_0 &+ \beta_{11}x_{1i} + \beta_{12}x_{1i}^2 + \cdots + \beta_{1k_1}x_{1i}^{k_1} \\
&+ \beta_{21}x_{2i} + \beta_{22}x_{2i}^2 + \cdots + \beta_{2k_2}x_{2i}^{k_2} + \cdots \\
&+ \beta_{p1}x_{pi} + \beta_{p2}x_{pi}^2 + \cdots + \beta_{pk_p}x_{pi}^{k_p} + \varepsilon_i, \quad i = 1, \cdots, n,
\end{aligned}
\tag{1}
$$

where the error ε_i is a normal distribution with mean 0 and variance σ^2, $\varepsilon_i \sim N(0, \sigma^2)$. For the sake of brevity, Equation 1 is rewritten in a matrix form as

$$
Y = XB + \varepsilon, \quad \varepsilon \sim N(0, \sigma^2 I),
\tag{2}
$$

where

$$
B = \left[\beta_0, \beta_{11}, \cdots, \beta_{1k_1}, \beta_{21}, \cdots, \beta_{2k_2}, \cdots, \beta_{p1}, \cdots, \beta_{pk_p} \right]^T,
\tag{3}
$$

$$
X = \begin{bmatrix}
1 & x_{11} & \cdots & x_{11}^{k_1} & x_{21} & \cdots & x_{21}^{k_2} & \cdots & x_{p1} & \cdots & x_{p1}^{k_p} \\
1 & x_{12} & \cdots & x_{12}^{k_1} & x_{22} & \cdots & x_{22}^{k_2} & \cdots & x_{p2} & \cdots & x_{p2}^{k_p} \\
\vdots & \vdots & \ddots & \vdots & \vdots & & \ddots & \vdots & \ddots & \vdots & \ddots & \vdots \\
1 & x_{1n} & \cdots & x_{1n}^{k_1} & x_{2n} & \cdots & x_{2n}^{k_2} & \cdots & x_{pn} & \cdots & x_{pn}^{k_p}
\end{bmatrix}, Y = \begin{bmatrix} y_1 \\ y_2 \\ \vdots \\ y_n \end{bmatrix}, \varepsilon = \begin{bmatrix} \varepsilon_1 \\ \varepsilon_2 \\ \vdots \\ \varepsilon_n \end{bmatrix},
\tag{4}
$$

and I denotes the unit matrix of dimension n. The density form of Equation 2 can be expressed as

$$f\left(Y \mid X, B, \sigma^2\right) = \frac{1}{(2\pi\sigma^2)^{n/2}} \exp\left[-\frac{(Y-XB)^T(Y-XB)}{2\sigma^2}\right]. \tag{5}$$

In the GLM, the unknown parameters in the model are the coefficient vector B and the regression variance σ^2.

When Bayesian inference is applied to the GLM, a prior distribution should be specified for each model parameter (e.g., the intercept, linear slope, and quadratic slope). Priors are helpful for incorporating information (or uncertainty) about the model parameters in addition to that provided by the monitoring data. These priors often take the form of a known probability distribution, e.g., the normal distribution. According to the level of (un)certainty in prior, the priors can be informative and noninformative (e.g., diffuse priors), the former representing the high degree of certainty about the parameter values while the latter bearing very litter certainty (or knowledge). In this study, the normal inverse-gamma prior that is the natural conjugate prior for Bayesian regression inference is used, that is,

$$f\left(B, \sigma^2\right) = f\left(B \mid \sigma^2\right) f\left(\sigma^2\right). \tag{6}$$

with

$$f\left(B \mid \sigma^2\right) = N\left(B_0, \sigma^2 \Sigma_0\right) = \frac{1}{(2\pi\sigma^2)^{k/2} \cdot \left|\sum_0\right|^{1/2}} \exp\left[-\frac{(B-B_0)^T \sum_0^{-1}(B-B_0)}{2\sigma^2}\right], \tag{7}$$

$$f\left(\sigma^2\right) = IG\left(\frac{a}{2}, \frac{b}{2}\right) = \frac{\left(\frac{b}{2}\right)^{a/2}}{\Gamma\left(\frac{a}{2}\right)} \left(\sigma^2\right)^{-a/2-1} \exp\left(-\frac{b}{2\sigma^2}\right), \tag{8}$$

where $IG(\cdot)$ represents the inverse-gamma distribution; B_0, Σ_0, a, and b can be determined based on the prior information stemming from an earlier data analysis, the expert knowledge, or the published literature.

According to Bayes' theorem, the posterior distribution of B and σ^2, $f(B, \sigma^2 \mid Y, X)$, is obtained by combining the likelihood function $f(Y \mid X, B, \sigma^2)$ and the prior distribution $f(B, \sigma^2)$

$$f\left(B, \sigma^2 \mid Y, X\right) = f\left(B, \sigma^2\right) \times f\left(Y \mid X, B, \sigma^2\right), \tag{9}$$

which can be re-expressed as

$$f\left(B, \sigma^2 \mid Y, X\right) = f\left(B \mid \sigma^2, Y, X\right) \times f\left(\sigma^2 \mid Y, X\right), \tag{10}$$

where

$$f\left(B \mid \sigma^2, Y, X\right) \sim N\left(B^*, \sigma^2 \sum{}^*\right), \; f\left(\sigma^2 \mid Y, X\right) \sim IG\left(\frac{a^*}{2}, \frac{b^*}{2}\right). \tag{11}$$

with

$$\sum{}^* = \left(X^T X + \sum_0{}^{-1}\right)^{-1}, \; B^* = \left(X^T X + \sum_0{}^{-1}\right)^{-1}\left(X^T Y + \sum_0{}^{-1} B_0\right), \tag{12}$$

$$a^* = a + n, \; b^* = b + Y^T Y + B_0{}^T \sum_0{}^{-1} B_0 - B^*\left(\sum{}^*\right)^{-1} B^*. \tag{13}$$

Note that Equation 10 is again the kernel normal inverse-gamma distribution, being factored as the conditional posterior distribution of B multiplied by the marginal posterior distribution of σ^2. In order to get the marginal posterior distribution of B, σ^2 has to be eliminated through integrating the following equation:

$$f(B\,|\,Y,X) = \int_0^\infty f\left(B,\sigma^2\,|\,Y,X\right)d\sigma^2. \tag{14}$$

The main stumbling block of Bayesian inference is the solution of posterior distribution of B as it involves high-dimension integration which is not analytically tractable. A variety of sampling-based methods, termed Markov chain Monte Carlo (MCMC) methods, have been developed to deal with this obstacle regardless of the number of parameters and complexity of the model. As one of the MCMC algorithms, Gibbs sampler has been commonly used since its inception to Bayesian statistics in 1990.[32] It is favorable for scenarios when sampling from a multivariate posterior is infeasible, but rather sampling from the conditional distributions for each variable is feasible. The basic rationale behind the Gibbs sampler is to generate a sample from the distribution of each variable in turn, conditional on the current values of other variables. The detailed iterative procedures of the Gibbs sampler are available in Ni et al.[17]

2.2 | Optimal model-class selection

One commonly encountered problem in statistical modeling is how to determine the best/optimal model class. Although a more complicated model structure can fit the data better than a less complicated one with fewer adjustable parameters, it is likely to lead to over-fitting. An over-fitted model may give rise to very poor results in prediction. Thus, the selected model class should attain a compromise between the accuracy and complexity. Put simply, the resulting model needs to fit well with the observed data and be as simple as possible. Bayesian model class selection (BMCS) is essentially the Bayesian updating at model class level through comparisons among alternative candidate model classes.[20] It has been recognized that a comparison between model classes should take into account not only the quality of data fitting but also the complexity of model. Consider a set $\mathcal{C} = \{C_1, C_2, \cdots C_{N_c}\}$ of N_c candidate models in Bayesian modeling. For each model C_j, the posterior distribution of model parameters (B, σ^2) given observation data Y is defined via Bayes' theorem:

$$f\left(B, \sigma^2 | Y\right) = \frac{f(Y|B, \sigma^2)f(B, \sigma^2)}{f(Y)}, \tag{15}$$

where $f(Y|B, \sigma^2)$ and $f(B, \sigma^2)$ are the likelihood function and joint prior distribution; $f(Y)$ is the marginal likelihood (or called evidence) which is our utmost concern as the probability of a model class is dominated by its evidence. Gull[33] demonstrated that the evidence has dual functionality of "achieve good data fitting" and "penalize complex models." Thus, Bayes' theorem about model class automatically incorporates a principle of model parsimony without the use of any ad hoc concepts.[34] The natural logarithm of the marginal likelihood (evidence) is

$$\ln f(Y) = \ln f\left(Y|B, \sigma^2\right) + \ln f\left(B, \sigma^2\right) - \ln f\left(B, \sigma^2|Y\right). \tag{16}$$

When the three terms on the right-hand side of Equation 16 become available, the marginal likelihood $\ln f(Y)$ can be computed readily. In most cases, the expressions of the first two terms $\ln f(Y|B, \sigma^2)$ and $\ln f(B, \sigma^2)$ are known in advance and easily obtained. However, the third term $\ln f(B, \sigma^2|Y)$ is difficult to calculate since the exact form of the posterior distribution is often unknown. In this regard, Chib[35] proposed an algorithm to estimate the posterior using the output from the Gibbs sampler. Recalling Equation 10 with dropping X, the posterior distribution is

$$f\left(B, \sigma^2|Y\right) = f\left(B|\sigma^2, Y\right) \times f\left(\sigma^2|Y\right). \tag{17}$$

The first term $f(B|\sigma^2, Y)$ on the right-hand side of Equation 17 is the conditional posterior for the regression coefficients, which is a normal distribution with mean B^* and variance $\sigma^2 \sum^*$ given in Section 2.1.1 and is therefore available. The second term $f(\sigma^2|Y)$ can be evaluated using the weak law of large number,[36] that is

$$f\left(\sigma^2|Y\right) \approx \frac{1}{L_1}\sum_{i=1}^{L_1} f\left(\sigma^2|Y,B_i\right), \tag{18}$$

where B_i's $(i = 1,2,\cdots,L_1)$ represent the L_1 draws of the Gibbs sampler. Thus, the marginal likelihood (evidence) can be estimated as

$$\ln f(y) = \ln f\left(y|B,\sigma^2\right) + \ln f\left(B,\sigma^2\right) - \ln f\left(B|\sigma^2,Y\right) - \ln f\left(\sigma^2|Y\right). \tag{19}$$

2.3 | Sparse Bayesian learning

Sparse Bayesian learning (SBL) is a nonparametric machine learning approach in the Bayesian context that shares characteristics in common with support vector machine (SVM) but derives accurate prediction models utilizing fewer basis functions than a comparable SVM.[31,37] Its ability of sparse representation and accurate prediction is primarily due to the Bayesian setting where uncertainty is considered and "inactive" basis terms can be automatically pruned through introducing hyperparameters in prior distributions of the weight parameters.[37] Hence, SBL exempts from the problem of overfitting which often occurs in classical least-squares and penalized least-squares. In recent years, SBL has also become a powerful framework for probabilistic compressive sensing.[38-41] The basic rationale of SBL for regression inference is briefly introduced below. Given a data set of input-target pairs $\{x_i,y_i\}_{i=1}^N$, the targets $y = [y_1,y_2,...,y_N]^T$ are assumed from a function or model $f(x)$ with additive noises $\varepsilon = [\varepsilon_1, \varepsilon_2, ..., \varepsilon_N]^T$,

$$y = f(x) + \varepsilon. \tag{20}$$

A nonparametric approach for modeling $f(x)$ is linearly weighted sum of M basis (kernel) functions, given by

$$f(x) = w^T\Phi(x) = \sum_{i=1}^{M} w_i\phi_i(x), \tag{21}$$

where $\Phi(x) = [\phi_i(x), \phi_2(x), ..., \phi_M(x)]^T$ is the $N \times M$ "design" matrix whose columns comprise the complete set of M basis vectors; $w = [w_1, w_2, ..., w_M]^T$ is the associated weight vector. The sparse Bayesian framework assumes an independent zero-mean Gaussian noise with variance σ^2, giving a multivariate Gaussian likelihood of the target vector y,

$$p\left(y|w,\sigma^2\right) = \frac{1}{\sqrt{(2\pi\sigma^2)^N}}\exp\left(-\frac{1}{2\sigma^2}||y-w^T\Phi||\right). \tag{22}$$

The maximum likelihood estimation of the unknown parameters w and σ^2 from Equation 22 may lead to severe overfitting and to avoid this, a common practice is to impose addition constraints on these unknowns to obtain a simple model. In the Bayesian framework, this issue can be solved perfectly by defining a set of explicit priors over these unknown parameters, which is also the key of SBL and available only in Bayesian setting. A popular choice of the prior for the weight vector w is

$$p(w|\alpha) = \prod_{i=1}^{M} p(w_i|\alpha_i) = \prod_{i=1}^{M} \frac{1}{\sqrt{2\pi/\alpha_i}}\exp\left(-\frac{1}{2}\alpha_i w_i^2\right), \tag{23}$$

where $\alpha = [\alpha_1, \alpha_2, ..., \alpha_M]^T$ is a hyperparameter vector, each independent hyperparameter individually controlling the strength of the prior over its associated weight. Given α, the posterior distribution of the weight vector w conditioned on the data is given by combining the likelihood and prior within Bayes' theorem:

$$p\left(w|y,\alpha,\sigma^2\right)=\frac{p(y|w,\sigma^2)p(w|\alpha)}{p(y|\alpha,\sigma^2)},\tag{24}$$

where the posterior covariance and mean vector of the weights are $\Sigma = (A+\sigma^{-2}\Phi^T\Phi)^{-1}$, $\mu = \sigma^{-2}\Sigma\Phi^T y$, with $A = diag$ $(\alpha_1, \alpha_2, ..., \alpha_M)$. Most-plausible point estimator α_{MP} and σ^2_{MP} can be derived by maximizing $p(y|\alpha,\sigma^2)$ with respect to α and σ^2 via a type-II maximum likelihood procedure.[37–41] The iterative updating of the hyperparameters α and the noise level σ^2 typically leads many α_i's to diverge toward infinity, resulting in the posterior of the corresponding weights highly peaked at zero. This means that the related basis functions $\phi_i(x)$ are irrelevant and can be pruned from the model given in Equation 21. Thus, the SBL offers an automatic regularization approach to making sparsity come out through pruning irrelevant basis functions in the iteration process.[31,37]

3 | CASE STUDY

3.1 | Tsing Ma Bridge and its SHM system

The Tsing Ma Bridge (TMB) (Figure 1) located in Hong Kong is a long-span double-decked suspension bridge, carrying both road and rail traffic. The bridge spans the main shipping channel between the Tsing Yi Island and Ma Wan Island with a main span of 1377 m and a total length of 2132 m. The height of the two bridge towers is 206 m from the base level to the tower saddle. Since the TMB is built in an active typhoon region, it was frequently attacked by strong winds. After completing the bridge construction, a long-term SHM, named Wind And Structural Health Monitoring System (WASHMS), has been devised and implemented by the Hong Kong Special Administrative Region Highways Department to monitor the structural performance and health condition of TMB.[42,43]

As a long-span suspension bridge built in a typhoon-prone region, an understanding of its wind environment and wind effects is critical to secure structural and operational safety of the bridge under strong winds. As part of the WASHMS, a total of 14 GPS receivers have been deployed on several key components of the bridge, including the towers, main cables, and four sections of the bridge deck, to monitor the displacement responses of TMB in longitudinal, lateral, and vertical directions. Each tower at the top was equipped a pair of GPS receivers. The mid-main cable, middle of the Ma Wan side span, one quarter, one half, and three quarters of the main span were installed a pair of GPS receivers, respectively. To avoid the obstruction of signal receiving caused by vehicles, all the antennae of the GPS receivers on the bridge deck were mounted at a height of 4 m and with a view angle of above 15°. The sampling rate of GPS was 10 Hz. Figures 2 and 3 show the locations of GPS receivers at different portions.

FIGURE 1   Tsing Ma Bridge (TMB) in Hong Kong

The WASHMS for TMB includes a total of 6 anemometers, of which two ultrasonic anemometers are deployed at the mid-main span, two mechanical propeller-type anemometers at the middle of the Ma Wan side span, and two mechanical propeller-type anemometers on the top of the Tsing Yi tower and the Ma Wan tower, as shown in Figure 2. To eliminate the disturbance from bridge deck, the anemometers at the deck level were respectively installed on the south and north sides of the bridge deck via a boom of 9 m long extended from the outmost of the deck. The sampling rate was 2.56 Hz.

3.2 | SHM data preprocessing

Available for this study are the wind information and structural displacement responses collected by the WASHMS during typhoons hitting Hong Kong in 2011. According to the Hong Kong Observation (HKO), there were three typhoons (typhoons Haima, Nesat, and Nockten) of Signal No. 3 or above during 2011.[44] Having received the monitoring data, we firstly confirm the direction of winds and select the windward wind data for the subsequent analysis, since the wind data recorded by the anemometers at the leeward side are interfered by the bridge deck and cannot represent the true wind loads acting on the bridge. Figure 4 illustrates the wind rose diagrams with 10-min wind speed higher than 5 m/s during the three typhoons in 2011.

Turbulence intensity is an important parameter used to describe the characteristics of fluctuating winds, which can strongly affect the dynamic response of bridge to winds. For turbulence-induced buffeting, larger turbulence intensity gives rise to increased dynamic response.[45] Figure 5 shows the variations of turbulence intensity in the longitudinal, lateral, and vertical directions against mean wind speed. It is seen that the turbulence intensity generally decreases with mean wind speed for the three directions and tends to be stable when the wind speed is larger than 8 m/s. Although the turbulence intensity is obtained at the low winds (<18 m/s), it is still a certain reference value. By observing the
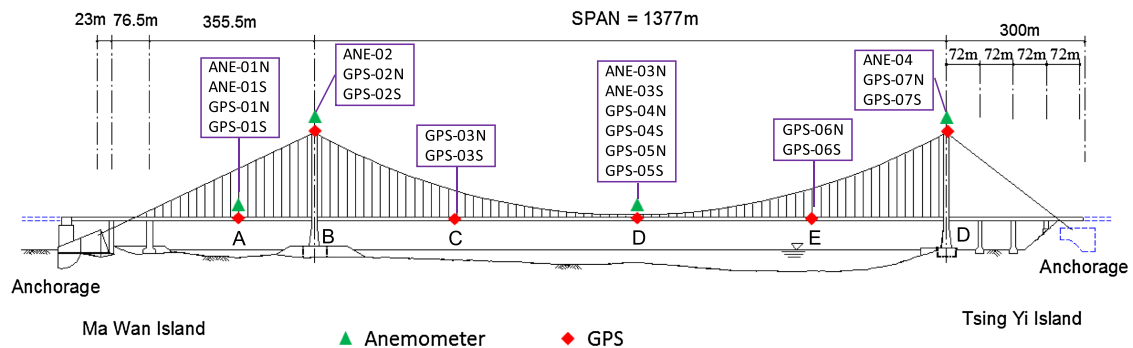

FIGURE 2 Layout of GPS receivers and anemometers on Tsing Ma Bridge (TMB)

FIGURE 3 GPS receivers deployed at different portions of the bridge: (a) tower top; (b) main cable; (c) deck
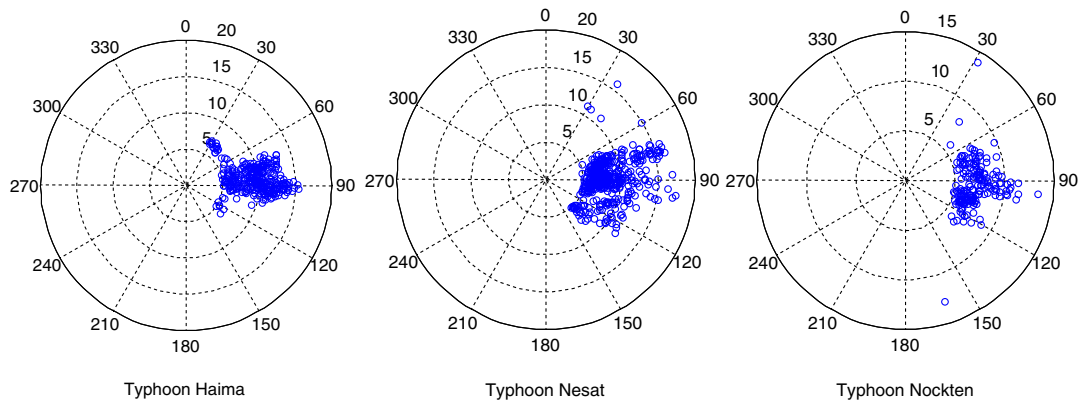
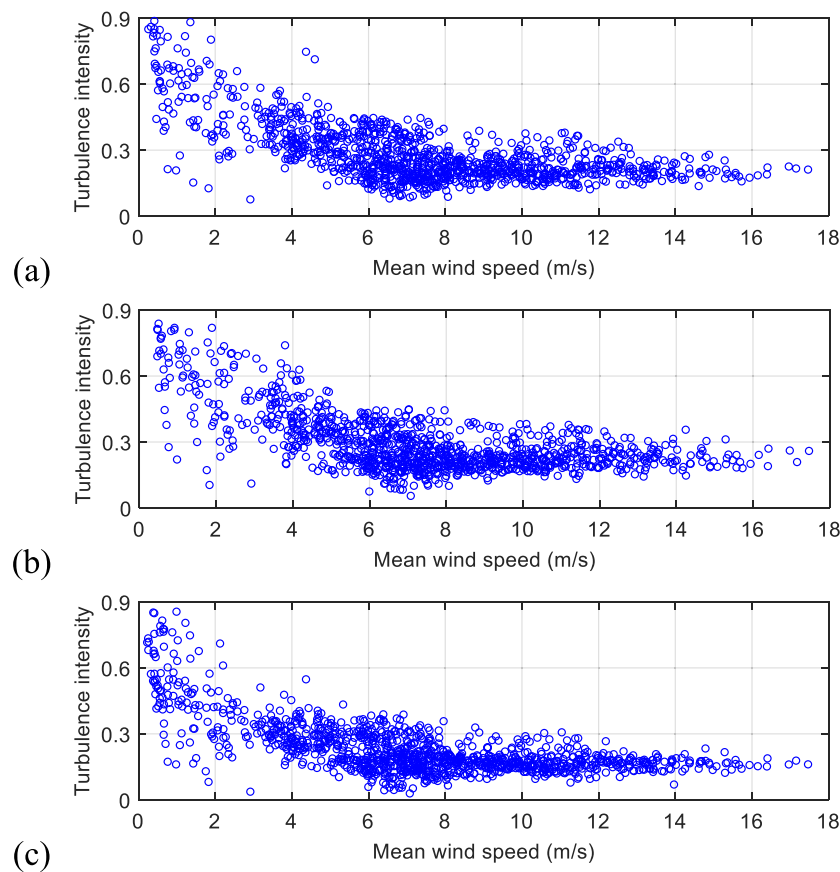**FIGURE 4** Wind rose diagrams obtained during three typhoons

FIGURE 5 Variation of turbulence intensity with mean wind speed: (a) longitudinal; (b) lateral; (c) vertical

trend, we can assume the turbulence intensity does not vary much between low (<18 m/s) and high wind speeds (>20 m/s).

To explore the relationship between the wind strength and displacement responses, the variations of the wind-induced displacement against mean wind speed in lateral, vertical and torsional directions are investigated. However, a good correlation between wind-induced displacement and mean wind speed can only be found in the lateral direction, which is consistent with the phenomenon observed by other researches.[6,14,15] So the wind-induced displacement in the lateral direction is investigated in this study.

The total displacement in the lateral direction can be decomposed into mean and dynamic components. The mean component is mainly affected by mean wind speed, while the dynamic component is mainly induced by both highway

load and dynamic wind load. The average standard deviation of the dynamic displacement response of the mid-main span over the period of high traffic flow rates with light wind is about 5 mm in the lateral direction, which is often small and can be disregarded when the wind speed is high.[46] In addition, the traffic would partly affect the aerodynamic characteristics of bridges and further affect the dynamic response, but the real impact is hard to quantify. To overcome this problem, peak dynamic displacement is introduced to quantify the dynamic component induced by both highway load and wind turbulence.

The magnitude and direction of wind speed may fluctuate violently over time in the case of typhoon or hurricane and the random wind turbulence shows nonstationary characteristics.[47] However, the general analysis methods for estimating wind-induced structural buffeting response are still based on the assumption of stationary wind excitations, which means that the average wind speed in a given time duration (e.g., 10 min) is thought to be steady and the wind fluctuation around its mean is a stationary random process. The total displacement response is defined as the mean displacement plus or minus the peak dynamic displacement for strong wind events, as follows:

$$\hat{D} = D \pm D_{max} = D \pm m\sigma_D, \tag{25}$$

where $\hat{D}$ is the wind-induced total displacement of the bridge deck and cable; D represents the wind-induced mean displacement; D_{max} is the peak dynamic displacement, which is defined as the standard deviation (σ_D) of displacement response multiplied by a statistical peak factor (m):

$$D_{max} = m\sigma_D. \tag{26}$$

Akin to gust factor, the value of m is defined as the ratio of the gust displacement within gust duration t_g (normally 3 s) to the 10-min mean displacement, as follows:

$$m = \frac{\max\left(d(\bar{t_g})\right)}{D}, \tag{27}$$

where $\max\left(d(\bar{t_g})\right)$ is the maximum mean wind-induced displacement during t_g, and D is the 10-min mean wind-induced displacement. Figure 6 shows the variation of the peak factor against the 10-min mean wind speed at different measurement positions. It is observed that the peak factor tends to keep in a narrow range at high wind speeds. The mean values of the peak factor at the mid-main cable (Section D), mid-main span (Section D), and 1/4 main span (Section C) are approximately 2.5.

Figure 7a,b illustrates the 10-min mean wind speed and wind direction, which were collected by the ultrasonic anemometer located at the mid-main span (Section D). Figure 7c–e shows the 10-min mean wind-induced total displacement responses in the lateral direction at the mid-main cable (Section D), mid-main span (Section D), and 1/4 main span (Section C), respectively. It is seen that the trends of wind speed and wind-induced displacement are roughly coincident.

3.3 | Verification of optimal Bayesian model

The GLM shown in Equation 1 is a general expression. For the problem concerned in this study, we are interested to obtain a more precise model by adding/erasing terms or by considering higher order. A good regression model should agree closely with the observed data but otherwise be as simple as possible. In this section, the BMCS approach is employed to select the best/optimal model by determining the number of polynomial terms and the polynomial order. According the previous study, the polynomial order is often no more than three.[6] Therefore, here we consider only the following three models whose highest order not exceeding four:

$$M_1 : y_i = \beta_0 + \beta_1 x_i + \beta_2 x_i^2 + \varepsilon_i,$$
$$M_2 : y_i = \beta_0 + \beta_1 x_i + \beta_2 x_i^2 + \beta_3 x_i^3 + \varepsilon_i,$$
$$M_3 : y_i = \beta_0 + \beta_1 x_i + \beta_2 x_i^2 + \beta_3 x_i^3 + \beta_4 x_i^4 + \varepsilon_i,$$
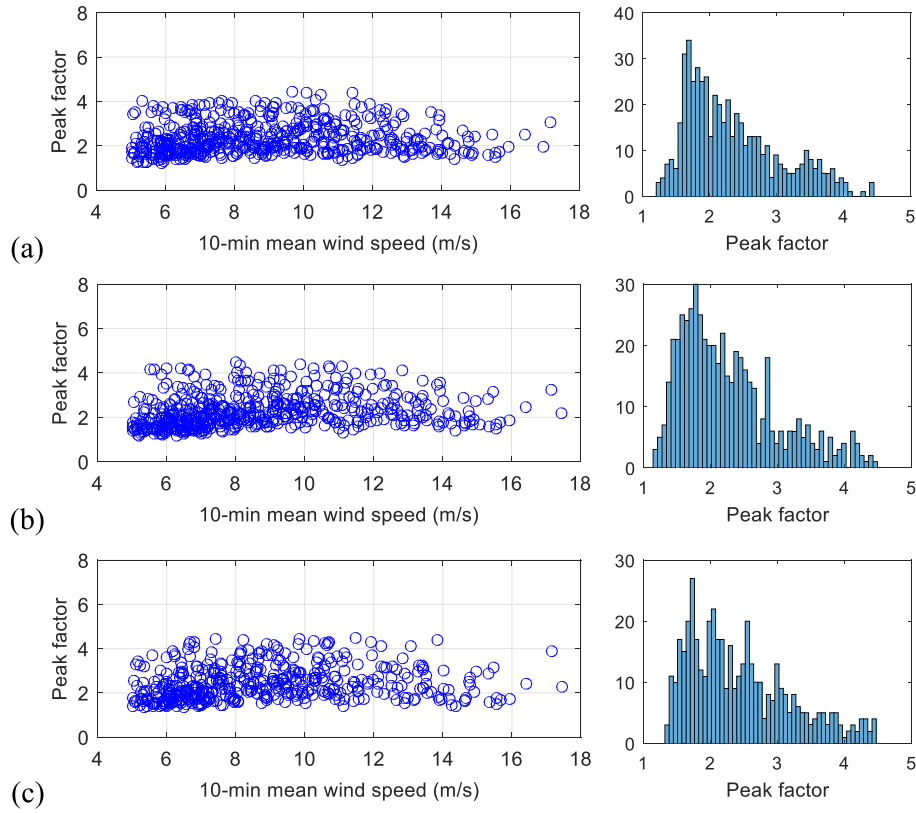
FIGURE 6   Peak factor at different positions: (a) mid-main cable; (b) mid-main span; (c) 1/4 main span

where M_1 depicts a quadratic polynomial model, M_2 is a cubic polynomial model, and M_3 is a quartic polynomial model. The BMCS approach is implemented to select the best/optimal one among the three models by evaluating $\ln f(y)$ in accordance with Equation 19. For convenience in comparing $\ln f(y)$ for datasets of different sizes, average log likelihood is used, defined as

$$\frac{LLH}{n} = \frac{\ln f(y)}{n}, \tag{28}$$

where n is the number of observations. The maximum of LLH/n is favored. In addition, root mean squared error (RMSE) is adopted to validate the accuracy of the established models, defined as

$$RMSE = \sqrt{\frac{\sum_{i=1}^{n}(y_i - \hat{y}_i)^2}{n}}, \tag{29}$$

where y_i and $\hat{y}_i$ are the measured and predicted values, respectively, and n is the number of observations.

In sparse Bayesian regression modeling, we design the matrix $\Phi(x)$ in Equation 21 as follows:

$$\Phi(x) = \left[x_1^0, x_1^{0.05}, x_1^{0.1}, ..., x_1^4, x_2^0, x_2^{0.05}, x_2^{0.1}, ..., x_2^2\right]^T, \tag{30}$$

where x_1 and x_2 represent the wind speed and wind direction, whose exponentials are set as $[0 : 0.05 : 4]$ (81 terms in total) and $[0 : 0.05 : 2]$ (41 terms in total), respectively. Thus, the "design" matrix $\Phi(x)$ has a total of 122 basis functions. The SBL model considering both wind speed and wind direction as explanatory variables becomes

$$M_4 : y = [w_1, w_2, ..., w_{122}]^T \left[x_1^0, x_1^{0.05}, x_1^{0.1}, ..., x_1^4, x_2^0, x_2^{0.05}, x_2^{0.1}, ..., x_2^2\right]^T + \varepsilon.$$
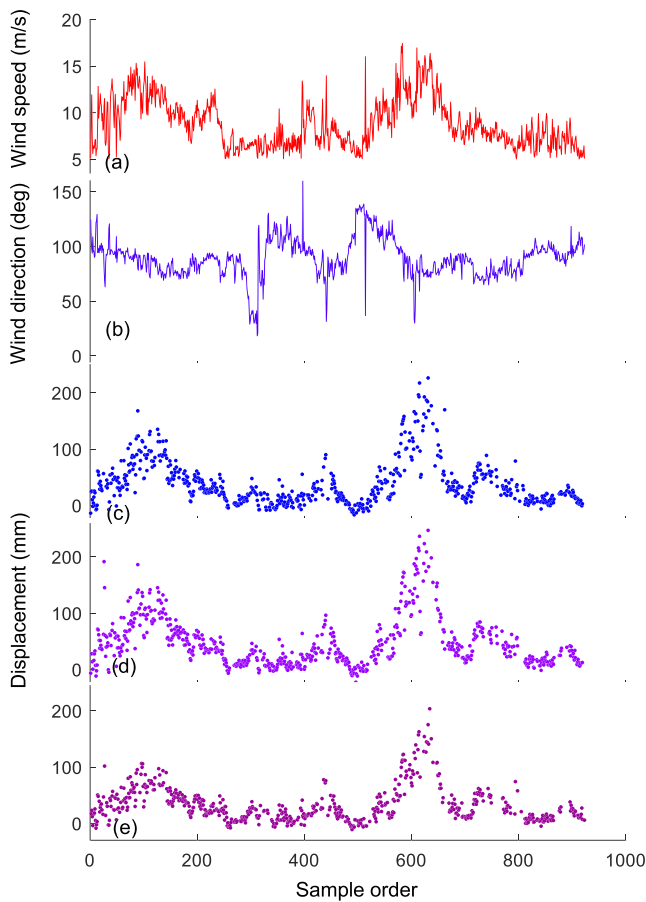
FIGURE 7 Sequences of measured wind speed, wind direction and wind-induced total displacement in lateral direction: (a) wind speed; (b) wind direction; (c) displacement at mid-main cable; (d) displacement at mid-main span; (e) displacement at 1/4 main span

The objective is to find the values of the weight w such that responses y generalize well to the new data yet only a few components of w are nonzero. The optimal combination of basis vectors is automatically determined based on the nonzero components of w.

The measured data are divided into two groups: training data set (data obtained from typhoons Haima and Nesat) and testing data set (data obtained from typhoon Nockten). The BGLM and SBL model are formulated by using the training data, while the unseen testing data are used to evaluate the performance of the formulated models. In regard to the different locations (i.e., mid-main cable, mid-main span, 1/4 main span), a total of nine BGLMs and three SBL models are constructed with the use of the training data.

To obtain a clear picture of the reconstruction capacity of the formulated models, the LLH/n values of different BGLMs and the RMSE values of the BGLMs and SBL models are compared in Figure 8. Obviously, M_1 with the largest LLH/n and minimum RMSE is the optimal model among the three candidate BGLMs for each location, but its reconstruction capacity performs worse than M_4 (SBL model) in terms of RMSE score. To further verify the prediction performance of the formulated models on unseen data, the new data from typhoon Nockten is used for testing. The RMSE scores for the testing data obtained from different locations are illustrated in Figure 9. It is observed that there is no significant distinction between reconstruction capability and prediction capability for the formulated BGLMs and SBL models. Likewise, M_4 with the minimum RMSE score performs the best, followed by M_1. Figure 10 compares the residual distributions of predicted displacement in the training and testing phases by the models M_1 and M_4. It is seen that the residuals roughly conform to a normal distribution, but the residual distributions of M_4 are slightly more concentrated around zero. Again, it can be concluded that M_4 outperforms M_1.

Tables 1 and 2 respectively summarize the detailed information about the model parameters of M_1 and M_4 for mid-main cable, mid-main span, and 1/4 main span. It is found that M_4 gives rise to smaller model errors ($\sigma = 24.24, 26.75, 21.51$) than M_1 ($\sigma = 26.51, 30.13, 22.93$), which indicates that M_4 is relatively more accurate under the same monitoring data. It is seen in Table 2 that the nonzero terms of weights w are 54, 50, and 49 for the mid-main cable, mid-main, span and 1/4 main span, respectively, with the corresponding basis functions being $x_1^{2.65}$, $x_1^{2.45}$, and $x_1^{2.40}$. The results show that only wind speed is singled out for interpreting the wind-induced lateral displacement responses by SBL.
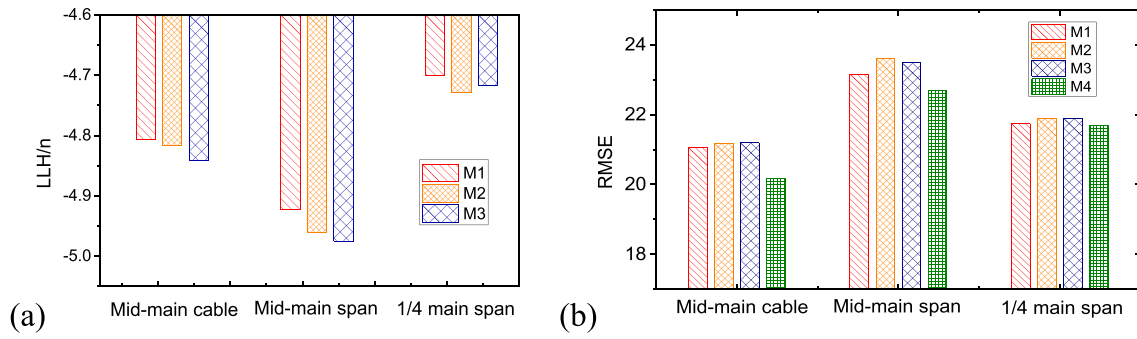
FIGURE 8 Comparison of reconstruction performance for different models: (a) LLH/n; (b) RMSE

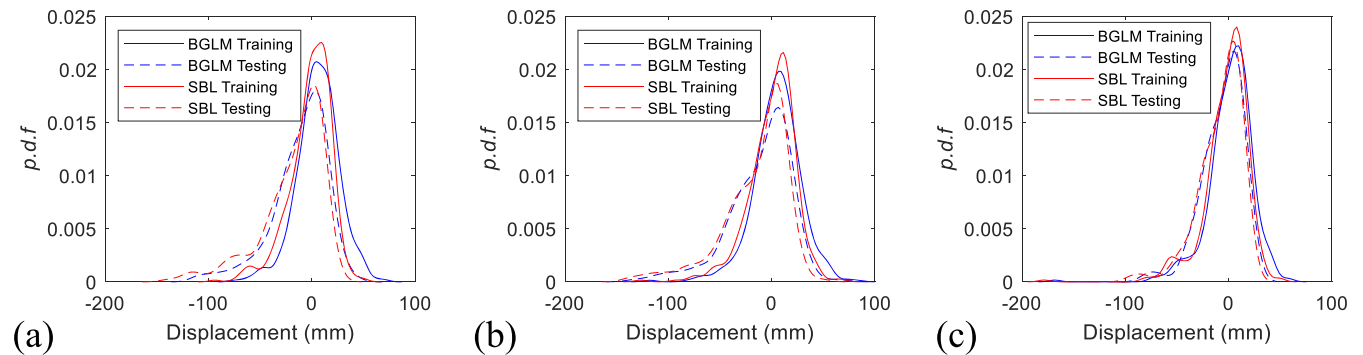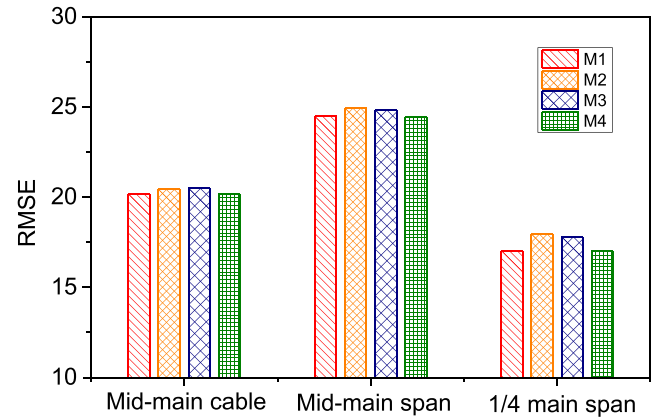**FIGURE 9** Comparison of prediction performance for different models

FIGURE 10 Residual distributions of predicted displacements in training and testing phases: (a) mid-main cable; (b) mid-main span; (c) 1/4 main span

3.4 | Performance assessment

Making use of the formulated BGLM (M_1) and SBL model (M_4), the bridge displacement responses at different structural portions under extreme wind events are then predicted for wind-resistant performance assessment of the bridge. Figures 11 to 13 illustrate the total lateral displacement responses under different 10-min mean wind speeds (including the design maximum wind speed), predicted by M_1 and M_4 for mid-main cable, mid-main span, and 1/4 main span, respectively. To facilitate wind-resistant performance assessment, the finite element method (FEM) analysis results of the lateral displacement responses of the bridge and the design maximum allowable total displacement at the serviceability limit state (SLS) are also provided for comparison. From these results, several observations are made:

TABLE 1 Estimated parameters of M_1

Location	Parameter	Mean	Standard deviation	95% confidence interval	
Mid-main cable	β_0	3.88	8.76	−13.30	20.91
	β_1	−3.99	1.78	−7.47	−0.51
	β_2	0.80	0.09	0.62	0.98
	σ	26.51	6.53	24.98	28.14
Mid-main span	β_0	2.47	9.04	−15.18	20.22
	β_1	−3.38	1.86	−7.04	0.25
	β_2	0.85	0.10	0.66	1.04
	σ	30.13	7.41	28.35	31.98
1/4 main span	β_0	4.89	8.59	−12.02	21.69
	β_1	−2.79	1.74	−6.18	0.61
	β_2	0.62	0.09	0.45	0.79
	σ	22.93	5.78	21.54	24.41

TABLE 2 Estimated parameters of M_4

Parameter	Mid-main cable	Mid-main span	1/4 main span
Nonzero component	54	50	49
Weight w	0.0741	0.1675	0.1363
Exponential	2.65	2.45	2.40
σ	24.24	26.75	21.51

i. As shown in Figures 11b, 12b, and 13b, the estimated most plausible displacements by M_1 (red curves) and M_4 (black curves) match well with the measured responses in low wind speed range (<18 m/s), and the majority of measurements lie within the 95% predictive interval except for some extrema.

ii. As most of the measurement data were obtained under wind speeds below 18 m/s, only FEM analysis results are available beyond the monitoring scope (wind speed > 20 m/s). With the FEM for simulating the buffeting-induced displacement response of TMB,[48] the total lateral displacement responses of the bridge at mid-main cable, mid-main span, and 1/4 main span have been obtained under different wind speeds (20, 30, 40, and 50 m/s), as plotted in Figures 11a, 12a, and 13a. It is seen that the most plausible total lateral displacement responses (red curves) estimated by M_1 under different wind speeds are smaller than those computed by FEM and the difference increases with the increase of wind speed, but all the computed results by FEM are within or close to the upper bound of the 95% confidence interval (CI). However, the most plausible total lateral displacement responses (black curves) predicted by M_4 are much closer to the FEM values and have a narrower CI. This means that M_4 has better prediction performance and lower prediction uncertainty than M_1. One salient advantage is that the two Bayesian models can be updated as more measurement data (especially those under wind speeds higher than 30 m/s) are available, enabling to yield an evolutionary wind-resistant performance assessment framework for a bridge instrumented with SHM system.

iii. For the TMB, the design 10-min mean wind speed at SLS is 53.3 m/s (equal to hourly-mean wind speed 50 m/s) for a 120-year return period and the maximum allowable total displacement response in the lateral direction is 2.9 m under the serviceability design wind speed.[16] Since the time period for collecting wind data on site is not long enough to examine the design wind speed for a 120-year return period, the design wind speed (53.3 m/s) is used here for preliminary wind-resistant performance assessment. By feeding the design wind speed into the formulated M_1 and M_4, the distributions of the predicted total lateral displacements at mid-main cable, mid-main span, and 1/4 main span are obtained as shown in Figures 11c, 12c, and 13c. It is seen that the total displacement responses at the mid-main cable in the lateral direction are close to that at the mid-main span, but both of them are larger than that at the 1/4 main span. Compared with those predicted by M_1, the displacement response distributions predicted by M_4 have larger mean values and smaller variances (lower uncertainty). The predicted mean displacement at the
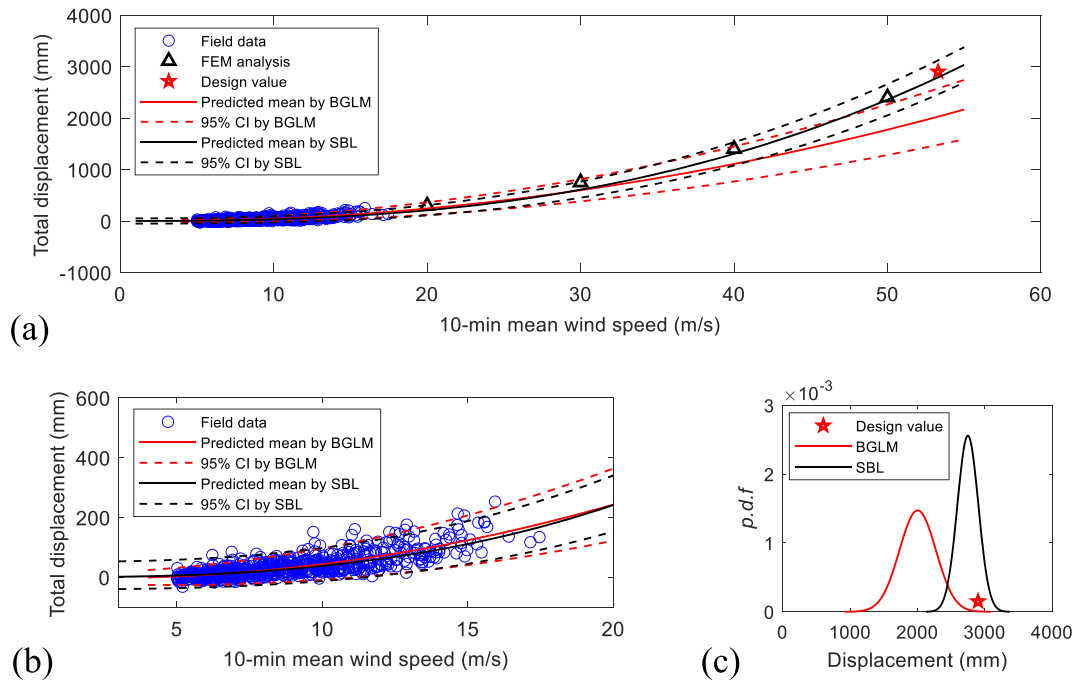
FIGURE 11 Forecast of responses at mid-main cable by BGLM and SBL: (a) comparison between estimation, FEM analysis, and design value; (b) relationship between 10-min wind speed and wind-induced total displacement in lateral direction; (c) distribution of predicted displacement response at design maximum wind speed
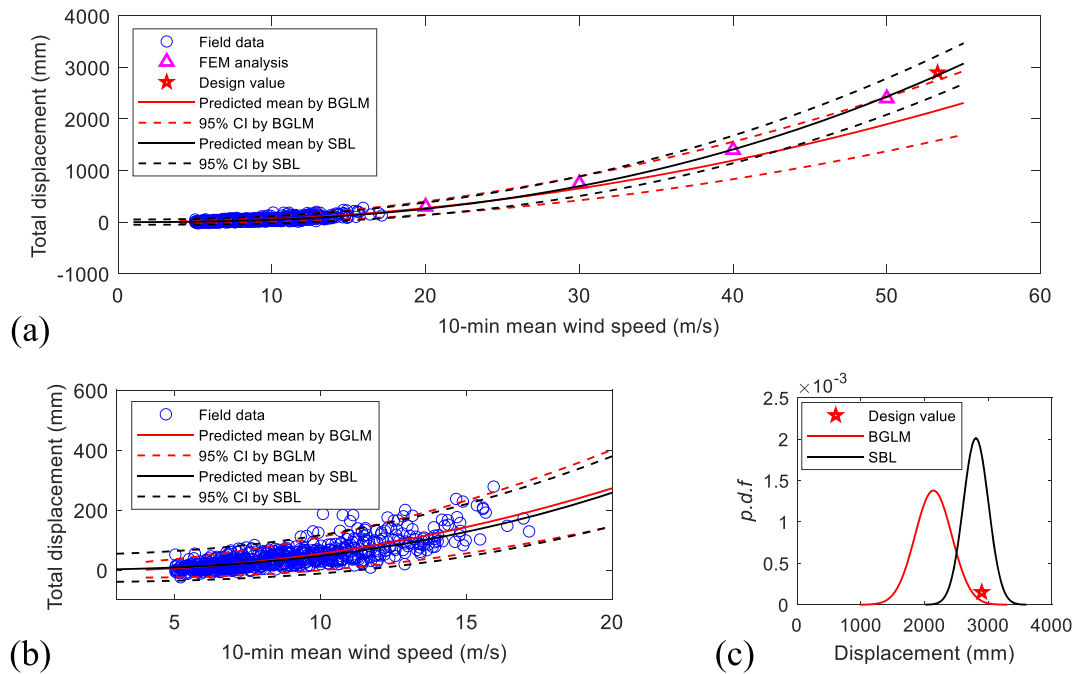

FIGURE 12 Forecast of responses at mid-main span by BGLM and SBL: (a) comparison between estimation, FEM analysis, and design value; (b) relationship between 10-min wind speed and wind-induced total displacement in lateral direction; (c) distribution of predicted displacement response at design maximum wind speed

mid-main span is 2.81 m by M_4, which is close to the maximum allowable total displacement response (2.9 m) according to the design criterion. On the contrary, the predicted mean displacement is only 2.18 m by M_1, far less than the design value. It testifies in one sense that the design is reasonable with appropriate safety reserve.
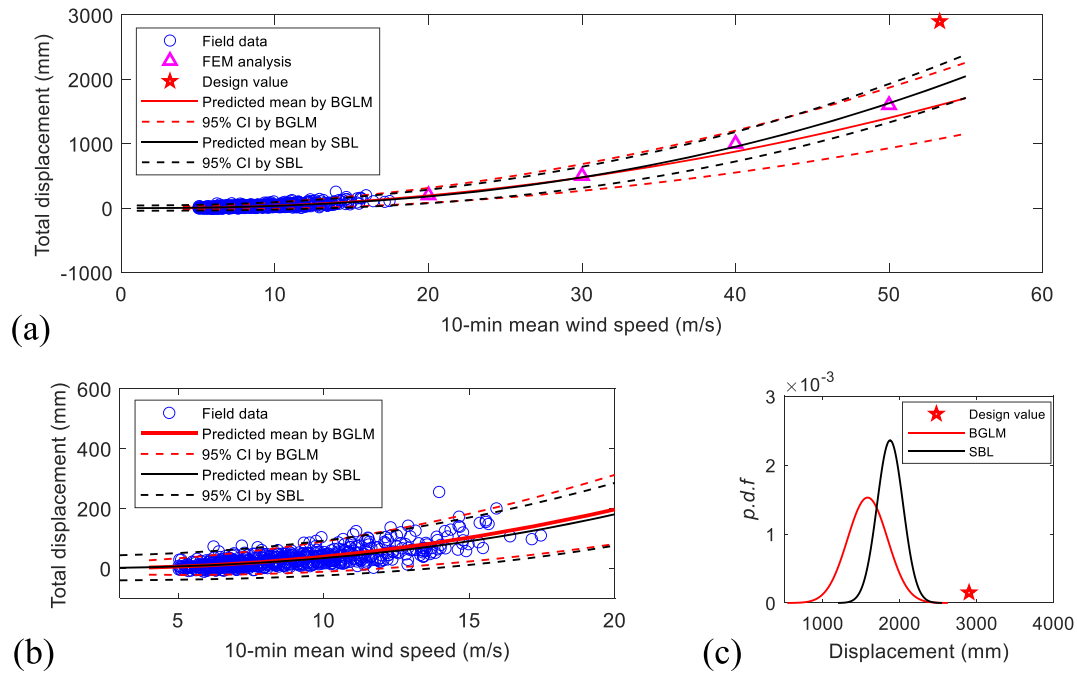
FIGURE 13 Forecast of responses at 1/4 main span by BGLM and SBL: (a) comparison between estimation, FEM analysis, and design value; (b) relationship between 10-min wind speed and wind-induced total displacement in lateral direction; (c) distribution of predicted displacement response at design maximum wind speed

iv. With the obtained posterior distribution, the displacement response with greatest probability or its probability for any given displacement response can be calculated. Such information including the prediction uncertainty (predictive interval) benefits the bridge management to prepare for the arrival of forthcoming strong typhoons, including decision making as to whether or when traffic on the bridge should be closed for the sake of safety according to the estimated displacement response as well as its corresponding probability by feeding the maximum wind speed forecasted by the observatory. Compared with other methods (e.g., FEM), the proposed BGLM and SBL methods enable to predict both the wind-induced displacement and its corresponding probability. Such probability approach is more sensible in assessing the wind-induced displacement because there are many types of modeling and parametric uncertainty in practice. During the typhoon, the wind characteristics, such as wind direction, wind turbulence intensity, and gust factor, exhibit high level of uncertainty. These uncertainties are assumed to be implicit in the model parameters and model error.

4 | CONCLUSIONS

Two probabilistic approaches, BGLM and SBL, for characterizing the wind-induced lateral displacement responses of long-span bridges have been proposed in the framework of Bayesian inference. They are model-free, data-driven approaches that do not need an FEM of the bridge and are preferable for reckoning the wind-induced total displacement for the purpose of wind-resistant performance evaluation. The optimal BGLM can be determined by incorporating the BMCS; while by means of SBL, the formulated probabilistic model exempts from overfitting and bears favorable generalization ability due to sparsity embedded by SBL.

The feasibility of the proposed methods has been verified by use of the monitoring data of wind speed, wind direction, and wind-induced displacement responses acquired from the suspension Tsing Ma Bridge. For each measurement location with monitoring data, three BGLMs (quadratic polynomial, cubic polynomial and quartic polynomial) are attempted to model the relationship between the 10-min mean wind speed and the wind-induced lateral displacement responses. By applying the BMCS criterion, the quadratic polynomial regression model (M_1) is identified as the optimal

model. In the SBL model (M_4), both wind speed and wind direction are used as explanatory variables; however, only wind speed is singled out for interpreting the wind-induced displacement responses by SBL. A comparison of RMSEs among different candidate models in both training and testing phases confirms that M_4 performs better than M_1. The wind-induced displacement responses estimated by M_4 at high wind speeds match well with the FEM analysis, while those predicted by M_1 are not very satisfactory. In particular, the predicted mean displacement of the mid-main span by M_4 (2.81 m) at the design maximum wind speed is close to the maximum allowable total displacement (2.9 m) stipulated in the design, whereas that predicted by M_1 (2.18 m) is much less than the design value.

It is worth mentioning that the proposed data-driven methods are unable to consider the difference in bridge aerodynamics (e.g., aerodynamic damping) at low winds and high winds. Due to the difference of bridge aerodynamics, the BGLM and SBL constructed using the data obtained under low winds may not fully represent the actual relationship between wind speed and wind-induced displacement at high winds. Whereas the BGLM and SBL could be updated once new monitoring data (especially those beyond the original monitoring scope) are available; thus an evolutionary wind-resistant performance assessment strategy can be executed for bridges instrumented with long-term SHM systems. The BGLM and SBL enable us not only to predict the most plausible wind-induced displacement at any wind speed (including extremely strong typhoons) but also to quantify the prediction uncertainty (predictive interval); such information is beneficial to bridge managers in making a proactive decision on whether to cease traffic on the bridge for the sake of safety when a strong typhoon is approaching.

ORCID

Y.W. Wang https://orcid.org/0000-0003-2293-4712
Y.Q. Ni https://orcid.org/0000-0003-1527-7777
Q.H. Zhang https://orcid.org/0000-0002-5776-5405

REFERENCES

1. Xu F, Chen A, Zhang Z. Aerostatic wind effects on the Sutong Bridge. *Proceedings of the 2013 Third International Conference on Intelligent System Design and Engineering Applications*. Hong Kong: 2013;247-256.
2. Vincent GS. Golden Gate bridge vibration studies. *Am Soc Civ Eng*. 1962;127(2):667-701.
3. Wang GX, Ding YL. Mathematical modeling for lateral displacement induced by wind velocity using monitoring data obtained from main girder of Sutong cable-stayed bridge. *Math Probl Eng*. 2014;2014:723152.
4. Green D, Unruh WG. The failure of the Tacoma Bridge: A physical model. *Am J Phys*. 2006;74(8):706-716.
5. Cheng J, Xiao RC. A simplified method for lateral response analysis of suspension bridges under wind loads. *Comm Numer Meth Eng*. 2006;22(8):861-874.
6. Chan WS. Application of GPS for monitoring long-span cable-supported bridges under high winds. *PhD Thesis*. Hong Kong: The Hong Kong Polytechnic University; 2009.
7. Kwon SD, Lee H, Lee S, Kim J. Mitigating the effects of wind on suspension bridge catwalks. *J Bridge Eng*. 2013;18(7):624–632.
8. Ashkenazi V, Roberts GW. Experimental monitoring of the Humber Bridge using GPS. *Civ Eng*. 1997;120(4):177-182.
9. Fujino Y, Murata M, Takeguchi M. Monitoring system of the Akashi Kaikyo Bridge and displacement measurement using GPS. *Proceedings of the SPIE's 5th Annual International Symposium on Nondestructive Evaluation of Highways, Utilities, and Pipelines*, Newport Beach, CA; 2000.
10. Wong KY. Instrumentation and health monitoring of cable-supported bridges. *Struct Control Health Monit*. 2004;11(2):91-124.
11. Koo KY, Brownjohn JMW, List DI, Cole R. Structural health monitoring of the Tamar suspension bridge. *Struct Control Health Monit*. 2013;20(4):609-625.
12. Xu L, Guo JJ, Jiang JJ. Time–frequency analysis of a suspension bridge based on GPS. *J Sound Vib*. 2002;254(1):105–116.
13. Mao JX, Wang H, Feng DM, Tao TY, Zheng WZ. Investigation of dynamic properties of long-span cable-stayed bridges based on one-year monitoring data under normal operating condition. *Struct Control Health Monit*. 2018;25(5):e2146.
14. Li H, Ou J, Zhao X, et al. Structural health monitoring system for the Shandong Binzhou Yellow River highway bridge. *Comput Aided Civ Inf Eng*. 2006;21(4):306–317.
15. Nakamura SI. GPS measurement of wind-induced suspension bridge girder displacements. *J Struct Eng*. 2000;126(12):1413–1419.

16. Xu YL, Chan WS. Wind and structural monitoring of long span cable-supported bridges with GPS. *Proceedings of the Seventh Asia-Pacific Conference on Wind Engineering*, Taipei, Taiwan; 2009.

17. Ni YQ, Wang YW, Zhang C. A Bayesian approach for condition assessment and damage alarm of bridge expansion joints using long-term structural health monitoring data. *Eng Struct*. 2020;212:110520.

18. Sohn H, Law KH. A Bayesian probabilistic approach for structure damage detection. *Earthq Eng Struct Dyn*. 1997;26(12):1259–1281.

19. Vanik MW, Beck JL, Au SK. Bayesian probabilistic approach to structural health monitoring. *J Eng Mech*. 2000;126(7):738–745.

20. Beck JL, Yuen KV. Model selection using response measurements: Bayesian probabilistic approach. *J Eng Mech*. 2004;130(2):192–203.

21. Ching J, Leu SS. Bayesian updating of reliability of civil infrastructure facilities based on condition-state data and fault-tree model. *Reliab Eng Syst Safety*. 2009;94(12):1962–1974.

22. Yuen KV. *Bayesian Methods for Structural Dynamics and Civil Engineering*. New York, USA: John Wiley & Sons; 2010.

23. Au SK, Zhang FL, Ni YC. Bayesian operational modal analysis: theory, computation, practice. *Comput Struct*. 2013;126:3–14.

24. Figueiredo E, Radu L, Worden K, Farrar CR. A Bayesian approach based on a Markov chain Monte Carlo method for damage detection under unknown sources of variability. *Eng Struct*. 2014;80:1–10.

25. Yuen KV, Huang K. Identifiability-enhanced Bayesian frequency-domain substructure identification. *Comput Aided Civ Inf Eng*. 2018;33(9):800–812.

26. Wan HP, Ni YQ. Bayesian modeling approach for forecast of structural stress response using structural health monitoring data. *J Struct Eng*. 2018;144(9):04018130.

27. Zhang LH, Wang YW, Ni YQ, Lai SK. Online condition assessment of high-speed trains based on Bayesian forecasting approach and time series analysis. *Smart Struct Sys*. 2018;21(5):705-713.

28. Lam HF, Hu J, Zhang FL, Ni YC. Markov chain Monte Carlo-based Bayesian model updating of a sailboat-shaped building using a parallel technique. *Eng Struct*. 2019;193:12–27.

29. Wang YW, Ni YQ, Wang X. Real-time defect detection of high-speed train wheels by using Bayesian forecasting and dynamic model. *Mech Syst Signal Process*. 2020;139:106654.

30. Wang YW, Ni YQ. Bayesian dynamic forecasting of structural strain response using structural health monitoring data. *Struct Control Health Monit*. 2020;27(8):e2575.

31. Ni YQ, Zhang QH. A Bayesian machine learning approach for online detection of railway wheel defects using track-side monitoring. *Struct Health Monit*. 2021. https://doi.org/10.1177/1475921720921772

32. Gelfand AE, Smith AFM. Sampling-based approaches to calculating marginal densities. *J Am Stat Assoc*. 1990;85(410):398-409.

33. Gull SF. Bayesian inductive inference and maximum entropy. In: Erickson G, Smith CR, eds. *Maximum-Entropy and Bayesian Methods in Science and Engineering*. Dordrecht, Netherlands: Springer; 1998.

34. Muto M, Beck JL. Bayesian updating and model class selection for hysteretic structural models using stochastic simulation. *J Vib Control*. 2008;14(1-2):7–34.

35. Chib S. Marginal likelihood from the Gibbs output. *J Am Stat Assoc*. 1995;90(432):1313-1321.

36. Koop G. *Bayesian Econometrics*. Chichester, United Kingdom: John Wiley & Sons Ltd; 2003.

37. Tipping ME. Sparse Bayesian learning and the relevance vector machine. *J Mach Learn Res*. 2001;1:211–244.

38. Babacan SD, Molina R, Katsaggelos AK. Bayesian compressive sensing using Laplace priors. *IEEE Trans Image Process*. 2010;19(1):53–63.

39. Huang Y, Beck JL, Wu S, Li H. Robust Bayesian compressive sensing for signals in structural health monitoring. *Comput Aided Civ Inf Eng*. 2014;29(3):160–179.

40. Lorintiu O, Liebgott H, Friboulet D. Compressed sensing Doppler ultrasound reconstruction using block sparse Bayesian learning. *IEEE Trans Med Imaging*. 2016;35(4):978–987.

41. Worley B. Scalable mean-field sparse Bayesian learning. *IEEE Trans Signal Process*. 2019;67(24):6314–6326.

42. Wong KY. Design of a structural health monitoring system for long-span bridges. *Struct Inf Eng*. 2007;3(2):169–185.

43. Ni YQ, Wong KY, Xia Y. Health checks through landmark bridges to sky-high structures. *Adv Struct Eng*. 2011;14(1):103–119.

44. Hong Kong Observatory (HKO). *Report of Tropical Cyclones in 2011*. Hong Kong; 2013.

45. Hua XG, Xu K, Wang YW, Wen Q, Chen ZQ. Wind-induced responses and dynamic characteristics of a super-tall building under a typhoon event. *Smart Struct Syst*. 2020;25(1):81–96.

46. Xu YL, Xia Y. *Structural Health Monitoring of Long-Span Suspension Bridges*. New York, USA: CRC Press; 2011.

47. Chen X, Kareem A. Equivalent static wind loads for buffeting response of bridges. *J Struct Eng*. 2001;127(12):1467–1475.

48. Liu TT, Xu YL, Zhang WS, Wong KY, Zhou HJ, Chan KWY. Buffeting-induced stresses in a long suspension bridge: structural health monitoring oriented stress analysis. *Wind Struct*. 2009;12(6):479–504.